

Self-Capacitance of High-Voltage Transformers

Luca Dalessandro, *Student Member, IEEE*, Fabiana da Silveira Cavalcante, *Student Member, IEEE*, and Johann W. Kolar, *Senior Member, IEEE*

Abstract—The calculation of a transformer's parasitics, such as its self capacitance, is fundamental for predicting the frequency behavior of the device, reducing this capacitance value and moreover for more advanced aims of capacitance integration and cancellation. This paper presents a comprehensive procedure for calculating all contributions to the self-capacitance of high-voltage transformers and provides a detailed analysis of the problem, based on a physical approach. The advantages of the analytical formulation of the problem rather than a finite element method analysis are discussed. The approach and formulas presented in this paper can also be used for other wound components rather than just step-up transformers. Finally, analytical and experimental results are presented for three different high-voltage transformer architectures.

Index Terms—Capacitance calculation, electrostatic analysis, high-voltage transformers.

I. INTRODUCTION

THE electrostatic analysis of wound components has been a fascinating research field since the beginning of last century when the study of the surge performance of transformers became an increasingly crucial issue for predicting the devices' frequency behavior [1], [2]. As soon as wideband transformers began appearing in telecommunication systems in the forties [3], [4], so followed papers devoted to the frequency characterization of these magnetic components [5] and, in particular, to the calculation of their self-capacitance [6]–[11]. The definition of a self-capacitance as a shunt lumped-element in the equivalent circuit of the wire-wound component is a very useful tool to justify and reproduce the first resonant frequency. However, the concept of self capacitance is well beyond any lumped-element circuit theory since it is an attempt to circumvent transmission line effects on wound-components when the current distribution begins to depart from its dc behavior [12], [13]. Recently, procedures for calculating the capacitance have been proposed for inductors [14], planar transformers [15], [16], magnetic components within SMPS [17], high-frequency transformers [18], [19] and power transformers [6], [7].

This paper presents a comprehensive procedure for calculating the self-capacitance of high-voltage transformers and identifies all the factors that dictate the electrostatic behavior of these components [37]. The typical application of high-voltage transformers is within isolated dc-to-dc converters, where they

step up the primary voltage and provide isolation [20]. For the high voltage transformer within a resonant dc-to-dc converter, where the switching frequency can rise up to 500 kHz [21], the parasitic parameters, in particular the self-capacitance, can heavily affect the performance of the converter. This capacitance is responsible for unwanted resonances and oscillations of the primary and secondary side currents, hence reducing the system's efficiency and reliability [22]. Thus the parasitics of the transformer, the leakage inductance and the parallel stray capacitance, have to be determined. These elements are usually used to form the resonant tank [23]. In order to predict the performance of the resonant converter and to be able to use the parasitics of the transformer as constitutive elements of the resonant circuit, the calculation of the stray capacitance is a fundamental issue [24].

The analytical approach was used instead of finite element method (FEM) analysis for two reasons. Firstly, in order to point out the physical relations of the electrostatics of wound components; secondly, to provide a simple and fast design tool that allows prediction rather than just reproduction of the capacitances. Moreover, the dependence of the capacitance value on the geometrical parameters and on the material properties is clearer when an analytical formulation of the problem is considered. On the other hand, numerical tools such FEM are able to model even complex structures and provide very accurate results, but at the cost of long simulation and overhead time required to draw the model and to set up the simulation parameters accurately. The FEM user might require some further time to learn a specific software package. Moreover, it is a good practice to verify the numerical results with another method, for instance an analytical one. Analytical tools are then a good tradeoff between speed to acquire results and their accuracy.

The main contributions to the self-capacitance in a high-voltage transformer whose secondary winding is divided into several sections made out of different layers of turns (see Fig. 1) are the following:

- a) the turn-to-turn capacitance;
- b) the layer-to-layer capacitance;
- c) winding-to-magnetic core;
- d) winding-to-electrostatic screen;
- e) interwinding interactions.

Although this paper addresses the calculation of the self-capacitance of step-up transformers, the analysis and the calculation procedure have general validity and the formulation can be adopted for other wound components.

The assumptions adopted herein for the calculation of the capacitance are as follows.

- a) Static electric field: the electric field E is independent of the magnetic induction B rate-of-change. The displacement current $\partial D/\partial t$ is as well neglected, and the problem is thus

Manuscript received February 2, 2006; revised August 4, 2006. Recommended for publication by Associate Editor B. Ferreira.

L. Dalessandro and J. W. Kolar are with the Power Electronic Systems Laboratory, Swiss Federal Institute of Technology (ETH) Zurich, Zurich CH-8092, Switzerland (e-mail: dalessandro@lem.ee.ethz.ch; kolar@lem.ee.ethz.ch).

F. da Silveira Cavalcante is with ABB Switzerland, Ltd., Turgi CH-5300, Switzerland (e-mail: cavalcante@lem.ee.ethz.ch).

Color versions of one or more of the figures in this paper are available online at <http://ieeexplore.ieee.org>.

Digital Object Identifier 10.1109/TPEL.2007.904252

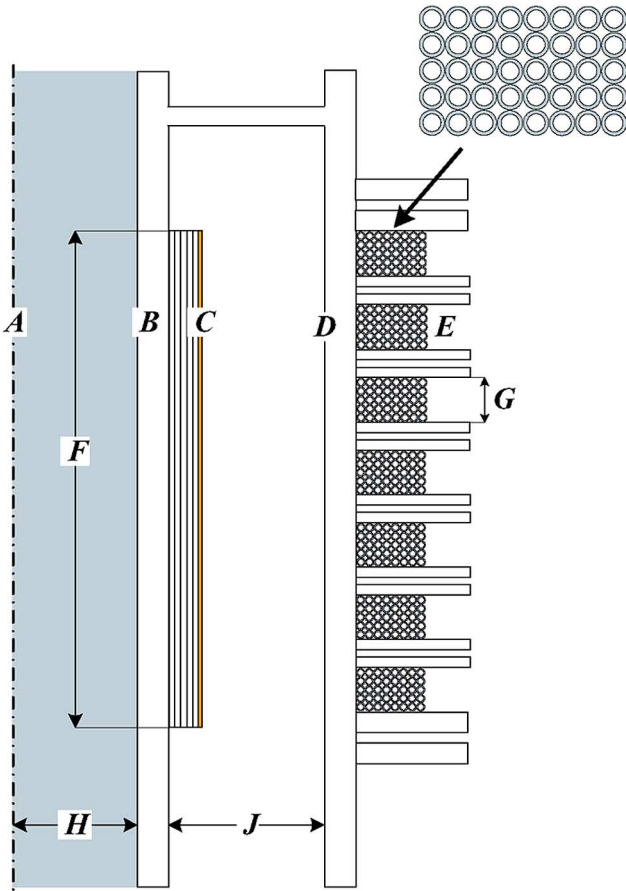


Fig. 1. Cross section of a high-voltage transformer. A: central axis of the transformer (cylindrical symmetry); B: insulating cylindrical coil-former for the primary winding; C: primary winding realized with a foil conductor and outer electrostatic screen; D: coil-former for the secondary winding divided in sections; E: section made out of several layers of turns. F: width of the primary; G: section's width; H: magnetic core's leg radius; and J: air-gap between windings.

time-independent. Accordingly, the incremental parasitic capacitance due to dynamic fields is neglected [25].

- b) No distributed charge between the electrodes. The volume charge ρ_T is neglected while only the surface charge σ_T is considered; this assumption and the previous one lead one to consider the equivalent winding like its dc or "electrostatic" equivalent.
- c) Uniform voltage distribution along the turns (equal magnetic flux linked to each turn) and all turns have the same length.

This paper is organized as follows. Section II describes the structure of the high voltage transformer and deals with the self-capacitance of the basic cell assumed for the calculations, the turn-to-turn capacitance. In Section III, the effect of the magnetic core on the electric flux lines distribution is analyzed and discussed. Afterwards, Section IV deals with the layer-to-layer electrostatic interaction and the calculations of the capacitance of the secondary winding and winding-to-screen are presented. Section V presents the experimental results obtained from three different high-voltage transformers, which validate the proposed procedure of calculation. Finally, Section VI summarizes and concludes.

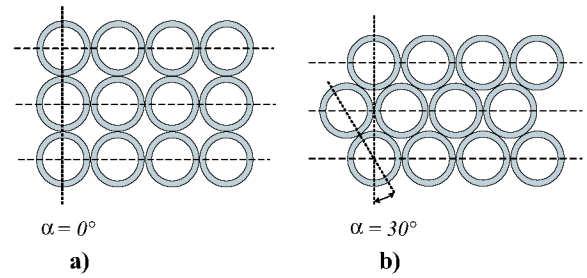


Fig. 2. Arrangements of turns: (a) conductors aligned and (b) orthocyclic or hexagonal turns grid.

II. BASIC CELL FOR THE CAPACITANCE CALCULATION

A. Transformer Characteristics

The typical high-voltage transformer's structure is depicted in Fig. 1. It is comprised of an E or U ferrite core and solid or Litz wire windings. The primary usually only has a few turns, realized by a foil conductor, while the secondary presents a larger number of turns, arranged in layers and split into several sections. The secondary coils are usually hosted within a dielectric coil-former that keeps the required distance between the windings parts and guarantees the electric breakdown limits with respect to the voltage level in operation. A grounded electrostatic screen is usually inserted between the windings in order to split and ground the interwinding capacitance. Furthermore, in order to increase the stepup ratio, the transformers are often built with multiple secondary windings, which are then series connected.

The three decisive factors that mainly affect the value of the self-capacitance are:

- a) the dielectric constant of the insulating materials interposed between the conductors;
- b) the geometry, i.e., diameter and dimension of the energized conductor, and the mutual spacing between wires and their distance to the screen or to the core;
- c) the winding arrangement and the strategy of connecting the different winding sections, which affect the distribution of the potential within each winding and between different windings and thus the amount of electrostatic energy stored (see Fig. 2).

B. Single Turn Capacitance

Whenever an energized wire is in the proximity of another wire or of a ground plane, the electric field lines leaving the wire terminate on the surrounding conductors and they are distributed in the space such that the Laplace's equation

$$\nabla^2 \varphi = 0$$

is satisfied.

The turn-to-turn capacitance or the turn-to-ground (core or screen) capacitance are the elementary cells for the analysis of the electrostatic behavior of a wound component. For a cell constituted by two turns, the two conductors represent the electrodes and the electric field lines are distributed within the interposed dielectric and air. The wire can be solid or composed by several twisted strands. In this latter case, if t_w and t_L indicate

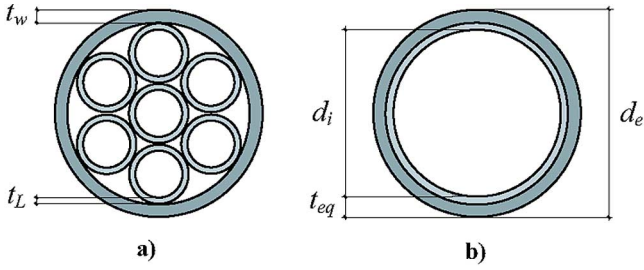


Fig. 3. Cross section of (a) a Litz wire. To determine (a) the equivalent isolation, the outer and the inner coating are considered as an equivalent dielectric of thickness t_{eq} and permittivity ε_{eq} .

the outer insulation thickness and the coating of each strand respectively [see Fig. 3(a)], then the equivalent dielectric constant ε_{eq} for a Litz wire is given by

$$\varepsilon_{eq} = \frac{\varepsilon_w \varepsilon_L (t_w + t_L)}{\varepsilon_L t_w + \varepsilon_w t_L} \quad (1)$$

where ε_w and ε_L are the dielectric constants of the outer insulation and of the coating of each strand, respectively. The equivalent insulation thickness is provided by

$$t_{eq} = t_w + t_L. \quad (2)$$

If the diameter d_L of each strand of a Litz wire is known, the outer diameter of the wire can be calculated as

$$d_e = d_L \sqrt{\frac{4N_s}{\pi}} \quad (3)$$

where N_s is the number of strands [26].

In order to calculate the capacitance, it is first necessary to derive the electric field distribution, given the potential field φ (boundary conditions). For the elementary cell, such as the one depicted in Fig. 4(a), the electric field E along an electric flux line l_{PQ} is given by

$$\int_P^Q E \cdot dl = \Delta\varphi_{PQ} \quad (4)$$

where $\Delta\varphi_{PQ}$ is the voltage difference between the two points. Once that E is calculated, the value of the corresponding capacitance C can be derived from the electrostatic energy stored in the volume Vol between the conductors

$$C = \frac{1}{\Delta\varphi^2} \int_{Vol} \varepsilon_{eq} E^2 dv. \quad (5)$$

Accordingly, the expression of the capacitance per unit of length for a single wire of circular cross section, uniformly charged, is given by

$$C_t = \varepsilon_0 \varepsilon_{eq} \frac{2\pi}{\ln\left(\frac{d_e}{d_i}\right)} \quad (6)$$

where $\varepsilon_0 = 8.854$ pF/m is the air permittivity, ε_{eq} is provided by (1), d_i and d_e are the inner and outer diameters [see Fig. 3(b)], respectively.

C. Basic Cell: Turn-to-Turn Capacitance

Equation (6) overestimates the value of the capacitance between two conductors because it is derived under the assumption that the charge is uniformly distributed over the surface of the

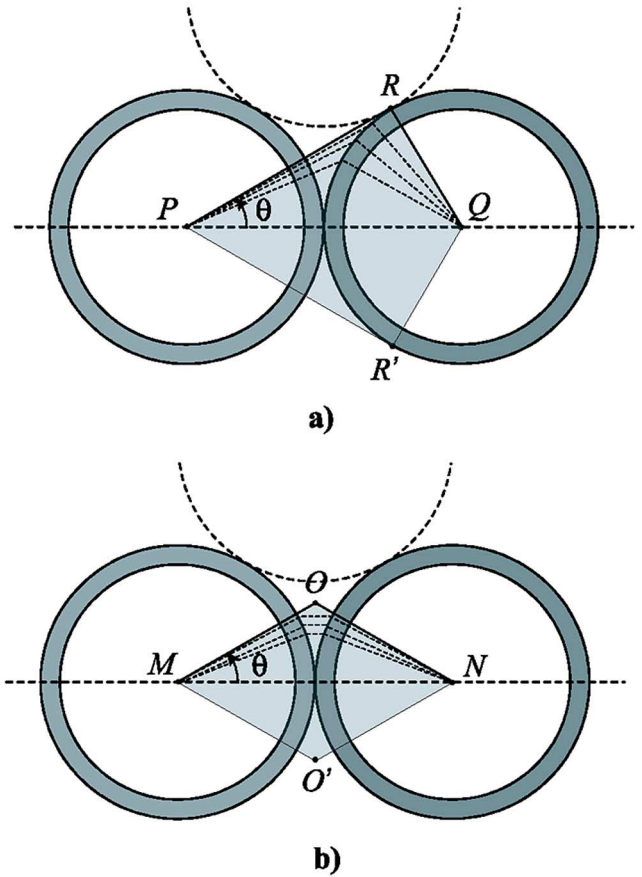


Fig. 4. Basic cells for the calculation of the turn-to-turn capacitance. According to Koch's approach, (a) the electric field lines are assumed radial, until they reach the surface of the adjacent turn, [27]. The integration path proposed by Massarini [14] is shown in (b): the electric field lines follow the shortest path in the air-gap between two adjacent turns.

conductor. In a real system, however, the charge tends to gather along portions of turns that are closest to neighboring turns. Therefore, in order to take into account a more realistic charge distribution, the electric field between two wires can be derived considering field integration paths closer to the actual electric flux lines configuration. With this in mind, one can suppose either that the electric field lines remain radial until they reach the surface of the adjacent turn [see Fig. 4(a)] or that they follow the shorter path in the air-gap between the turns [see Fig. 4(b)].

These two problems have already been faced by Koch [27] and Massarini [14], respectively. The calculation of the turn-to-turn capacitance corresponding to the configuration in Fig. 4(a) leads to the following formula:

$$C_{tt,K} = 2\varepsilon_0 \left(m_L + \frac{2t_{eq}}{\varepsilon_{eq}d_e^2} (d_e - t_{eq})m_D \right) \quad (7)$$

where the coefficients m_L and m_D are given, respectively, by

$$m_L = \int_0^{\frac{\pi}{6}} \frac{\frac{1}{2} - \left(\sin^2 \theta + \cos \theta \sqrt{\cos^2 \theta - \frac{3}{4}} \right)}{\left[\cos \theta - \left(1 - \frac{2t_{eq}}{\varepsilon_{eq}d_e} \right) \left(\frac{1}{2} + \sqrt{\cos^2 \theta - \frac{3}{4}} \right) \right]^2} d\theta,$$

$$m_D = \int_0^{\frac{\pi}{6}} \frac{\sin^2 \theta + \cos \theta \sqrt{\cos^2 \theta - \frac{3}{4}}}{\left[\cos \theta - \left(1 - \frac{2t_{eq}}{\varepsilon_{eq}d_e} \right) \left(\frac{1}{2} + \sqrt{\cos^2 \theta - \frac{3}{4}} \right) \right]^2} d\theta.$$

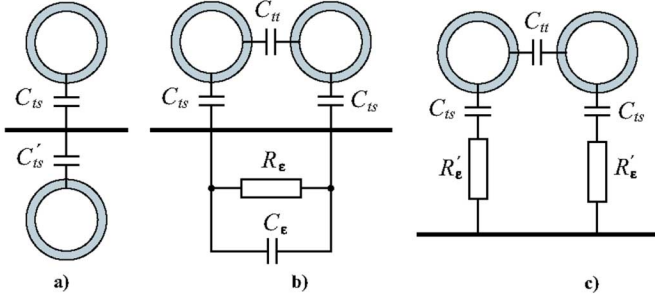


Fig. 5. (a) Wire to conductive-plane capacitance calculable with the method of images. (b) The properties of the core can be included in the model as a lossy capacitance or (c) as series resistors to the core [28].

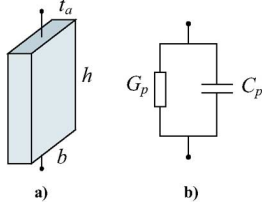


Fig. 6. (a) Sample shape for measuring the dielectric and conductive properties of ferrite and (b) its equivalent circuit. The parallel capacitance C_p and dielectric loss factor $\tan \delta_\epsilon$ (or D) of a thin ferrite slab for N87 ferrite, having dimensions of $8 \text{ mm} \times 8 \text{ mm} \times 1.52 \text{ mm}$, have been measured using the AGILENT A294A dielectric test fixture.

If a three piecewise-linear path is considered, as illustrated in Fig. 4(b), then the resulting capacitance (per unit of length) is given by

$$C_{tt,M} = \epsilon_{\text{eq}} \theta^* \ln^{-1} \left(\frac{d_e}{d_i} \right) + \epsilon_0 \cot \frac{\theta^*}{2} - \epsilon_0 \cot \frac{\pi}{12} \quad (8)$$

where

$$\theta^* = \arccos \left(1 - \frac{1}{\epsilon_{\text{eq}}} \ln \left(\frac{d_e}{d_i} \right) \right).$$

III. INFLUENCE OF THE CORE ON THE ELECTRIC FIELD DISTRIBUTION

The simplest winding arrangement is constituted by a single-layer coil wrapped around the magnetic core. In this configuration, the electric flux lines leaving each turn terminate on the adjacent turns and on the core. The latter usually consists of a ferrite material with a certain conductivity σ . The assumption of considering the core as an ideal conductor is useful to calculate the value of the capacitance against the core. The method of images can be used [14] and the formulas for the turn-to-turn capacitance derived in the previous section can be applied [see Fig. 5(a)]. However, in order to predict the frequency behavior of the systems, it is opportune to include the resistance of the core in the model [see Fig. 5(b)].

An example of frequency analysis of ferrite wound components is in [28]. There, it is shown how the equivalent core resistance is responsible for the considerable damping of the frequency resonance peaks due to the self capacitance and leakage inductance of the winding (see Fig. 6). Thus, in order to verify

the impact of the core resistivity on the transformer's frequency behavior, the parameters of ferrite material of grade N87 [29] of the transformers cores analyzed in the experimental part of this work, have been extracted. For this reason, a ferrite sample between two electrodes has been considered to be a lossy capacitor [30], and the complex permittivity

$$\dot{\epsilon} = \epsilon_0 \epsilon_r = \epsilon_0 (\epsilon' - j\epsilon'') \quad (9)$$

describes the relationship between the electrical field, E , within the material and the electric flux density $D = \dot{\epsilon}E$. The real part of the complex permittivity, ϵ' , accounts for the electrical energy stored in the dielectric material while the imaginary part, ϵ'' , accounts for the conduction losses.

The tests have been carried out using a tiny slab of material N87 of dimensions $8 \text{ mm} \times 8 \text{ mm} \times 1.52 \text{ mm}$ with the electrodes plated onto opposite $8 \text{ mm} \times 1.52 \text{ mm}$ faces [31]. The capacitive admittance of each thin plate, whose expression is given by

$$Y_p = G_p + j\omega C_p \quad (10)$$

is measured using an AGILENT A294A precision impedance analyzer with its dielectric test fixture. The measured capacitive reactance is used to derive the frequency-dependent real part of the relative permittivity as follows:

$$\epsilon'(f) = \frac{h}{\epsilon_0 t_a b} C_p(f). \quad (11)$$

The measured dielectric loss factor, $\tan \delta_\epsilon$, defined as

$$\tan \delta_\epsilon = \frac{\epsilon''}{\epsilon'} = \frac{G_p}{\omega C_p} = \frac{\frac{\sigma t_a b}{h}}{\omega \frac{\epsilon_0 \epsilon' t_a b}{h}} = \frac{\sigma}{\omega \epsilon_0 \epsilon'} \quad (12)$$

provides information on both dielectric and ohmic losses, that cannot be empirically split. Actually, the former are dependent on the lossy component of the dielectric constant, ϵ''_r , while the latter on the conductivity of the ferrite. The imaginary part of the permittivity and the equivalent conductivity σ of the ferrite are given by

$$\epsilon'' = \tan \delta_\epsilon \epsilon' \quad (13)$$

$$\sigma = \omega \tan \delta_\epsilon \epsilon_0 \epsilon' = \omega \epsilon_0 \epsilon'' \quad (14)$$

The frequency plot of ferrite parameters (ϵ' , ϵ'' , σ) is shown in Fig. 7. The conductivity assumes a large value over all the considered frequency band [100 kHz–100 MHz] that is of interest for practical applications. The damping of the frequency resonance peaks and the larger values of the winding impedance over all the frequency bandwidth are due to the large value of the core resistivity, $1/\sigma$, that leads to a value of the core resistance R_ϵ of some $\text{k}\Omega$ [see Fig. 5(b)]. In particular, these effects are more relevant when the coil is directly wrapped on the core, such as the primary winding (see Fig. 1), but are negligible when the winding is far from the core or a screen is interposed between the core and the winding.

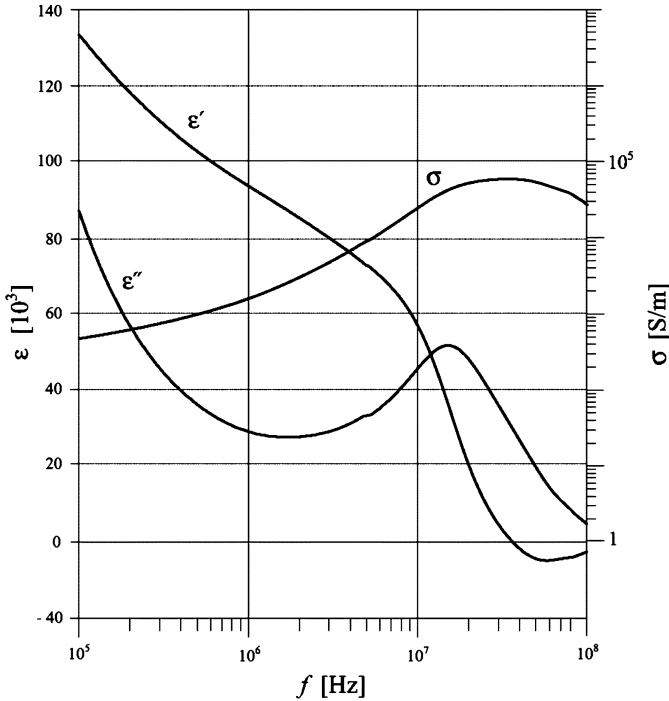


Fig. 7. Frequency plot of the real and imaginary parts ϵ' and ϵ'' of the complex relative permittivity and of the conductivity σ for N87 ferrite at 25 °C.

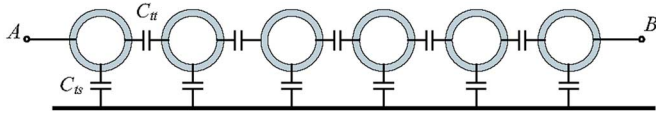


Fig. 8. Equivalent capacitance network for a single layer coil with a shield or core.

IV. CAPACITANCE OF THE SECONDARY WINDING AND CAPACITANCE TOWARDS SCREEN

A. Single Layer Capacitance

If the presence of a screen or core is considered, and if the capacitance between two nonadjacent turns is neglected, then the resulting equivalent network representing the distributed capacitances between adjacent turns, C_{tt} , and towards the screen, C_{ts} , can be seen as depicted in Fig. 8. In the simplest case, if the screen or core is distant from the coil or even absent (air-coil), the resulting capacitance C_{AB} across the terminals $A - B$ is given by

$$C_{AB} = \frac{C_{tt}}{n_t - 1} \quad (15)$$

where n_t is the number of turns. For the configuration depicted in Fig. 8, the resulting capacitance across the terminals is given by

$$C_{AB}(n_t) = \frac{C_{tt}}{2 + \frac{C_{tt}}{C_{AB}(n_t-2)}} + C_{tt} \quad (16)$$

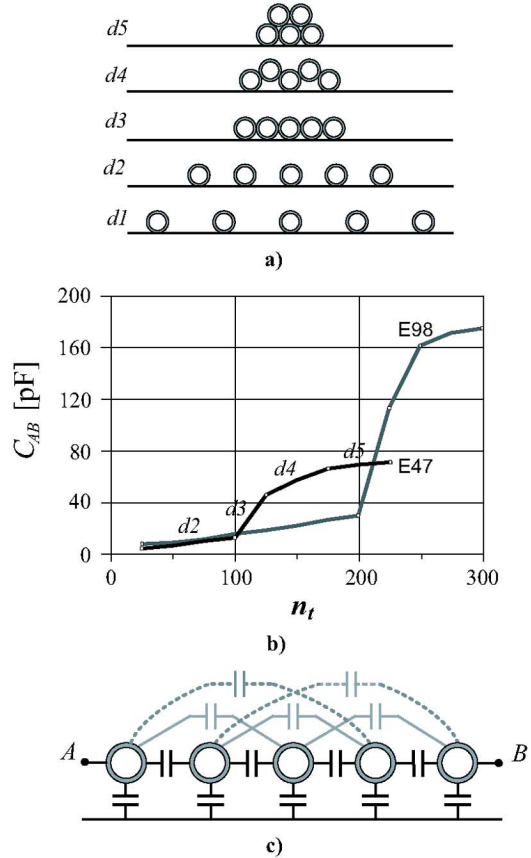


Fig. 9. Empirical verification of the dependence of the self capacitance of a single layer on the spacing between turns. (a) Different spacing between turns $d1 \dots d5$, (b) measured self-capacitance of a coil made out of a wire having a diameter of 0.5 mm and insulation thickness of 33 μm wound around two different cores, E47 and E98. n_t is the number of turns. (c) The electrostatic interactions between nonadjacent turns cannot be neglected for the configurations $d4$ and $d5$.

assuming the capacitance to shield C_{ts} is two times larger than the capacitance C_{tt} by virtue of the images method [see Fig. 5(a)]. Equations (15) and (16) have already been proposed in [14] and [32]. There, the capacitance C_{AB} depends inversely (15) and asymptotically, (16) on the number of turns, n_t . Both formulas provide good approximations of the self-capacitance if there are only a few turns or they are well spaced [see $d1$ Fig. 9(a)]. In the case of many turns, tightly wrapped around the core, the influence of the capacitive coupling between nonadjacent turns cannot be neglected and the dependence of C_{AB} on n_t is better expressed by a linear relationship [33], i.e., the capacitance increases linearly for increasing number of turns. Fig. 9(b) shows the relationship between the number of turns n_t and the measured capacitance C_{AB} for two different coils made with wire having a diameter of 0.5 mm with insulation thickness of 33 μm and magnetic cores, E47 and E98, of ferrite grade N87. For both cases the following behavior has been empirically registered. As long as the turns are wound uniformly, each turn close to the next one, a linear dependence of C_{AB} on n_t is observed [see $d2$ and $d3$ Fig. 9(a)]. In particular, the values of the capacitance measured for the two coils are nearly the same for fewer turns (see Fig. 9) because the cores have been

TABLE I
MEASURED AND CALCULATED WINDING CAPACITANCE [pF]

	Measured	Calculated with (7)	Calculated with (8)
Tr # 1	3.84	3.12	3.35
Tr # 2	4.84	4.22	4.47

wound with the same wire, although the E47 core had a further insulating coating with respect to the E98 core. For a larger n_t , the space between turns becomes tight, the turns start to overlap [see *d4* Fig. 9(a)] and a sudden increase of the capacitance C_{AB} is observed. This is because the electrostatic interaction between nonadjacent turns becomes stronger [see Fig. 9(c)]. As soon as the second layer begins to grow [see *d5* Fig. 9(a)], the dependence of C_{AB} on n_t is again linear and less steep, and the trend is the same as that registered for the first layer. This kind of dependence of C_{AB} on n_t can also be observed with more layers. It should be noted that the measurement in Fig. 9 could also have been equivalently realized by keeping the number of turns n_t constant while varying the mutual arrangement of the turns.

B. Layer-to-Layer Capacitance

Starting from the value of C_{tt} provided by (7) or (8) one can calculate the value of the capacitance between two layers of turns, then of a section of the winding constituted by z layers, and finally of the whole winding made out of q sections (see Fig. 1). Toward this aim the following formulas provide a good assessment of these capacitances [6]. The layer-to-layer capacitance C_{ll} is given by

$$C_{ll} = \frac{n_t(n_t + 1)(2n_t + 1)}{6n_t^2} l C_{tt} \quad (17)$$

where l is the average length of a turn. Then the capacitance C_s of a section is provided by

$$C_s = C_{ll}(z - 1) \left(\frac{2}{z}\right)^2. \quad (18)$$

Finally, for the overall winding, constituted by q sections, the capacitance is:

$$C_w = \frac{C_s}{q}. \quad (19)$$

Table I shows the calculated values of the secondary winding capacitances of transformers # 1 and # 2 whose specifications are given in the Appendix.

The use of (17) for calculating the layer-to-layer capacitance implies the calculation of the turn-to-turn capacitance C_{tt} by means of (7) or (8). This computational effort is worthwhile if the number of turns < 10 for layer, but for a larger number of turns it is convenient to use simpler formulas for calculating the capacitances. The winding structure can be modeled as a coaxial cylindrical capacitor, or if the curvature radius r is large (see Fig. 10), of a parallel plate capacitor:

$$C_{ll} = \varepsilon_0 \varepsilon_r \frac{2\pi w}{\ln\left(1 + \frac{d}{r}\right)} \xrightarrow{r \rightarrow \infty} C_{ll} = \varepsilon_0 \varepsilon_r \frac{2\pi r w}{d} \quad (20)$$

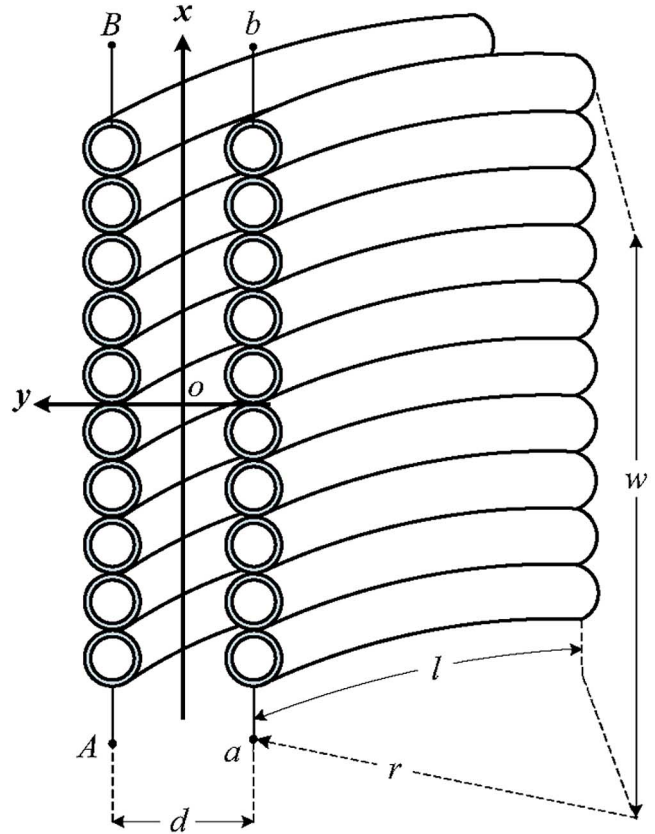


Fig. 10. Representation of two adjacent layers or single-layer windings.

where w is the width of the layer, or the breath of each section. Equation (20) is valid for a large number of turns with axial symmetry. For only a few spaced turns the calculation of C_{tt} by means of (7) or (8) has to be the basis for deriving the self-capacitance.

The value of the distance d between two wires of different layers plays a decisive role in the calculation of the capacitance. In general d is not provided by two times the insulation thickness (see Fig. 3), as one can easily and erroneously assume, but it is opportune to use an empirical formula [6] that accounts for the actual mutual position between wires, that are usually not perfectly aligned

$$d = 1.26 \cdot d_e - 1.15 \cdot d_i \quad (21)$$

where d_e and d_i are external and internal wire diameters, respectively, (see Fig. 3). Equation (21) should provide the length of the average electric flux line between two conductors rather than the insulation thickness. If the conductors are distant or the insulation is thick, then the actual distribution of electric flux lines can be more complex than the ones sketched in Fig. 4. Accurate information on the wire's characteristics, such as its insulation thickness and its cross-section, is very important in order to have a good assessment of the equivalent distance d and hence to reduce the error in the final calculation of the capacitance.

The expressions of the static capacitance C_{ll} (20) are derived under the assumption of uniform charge distribution over the conductors of each layer disconnected (see Fig. 10). However,

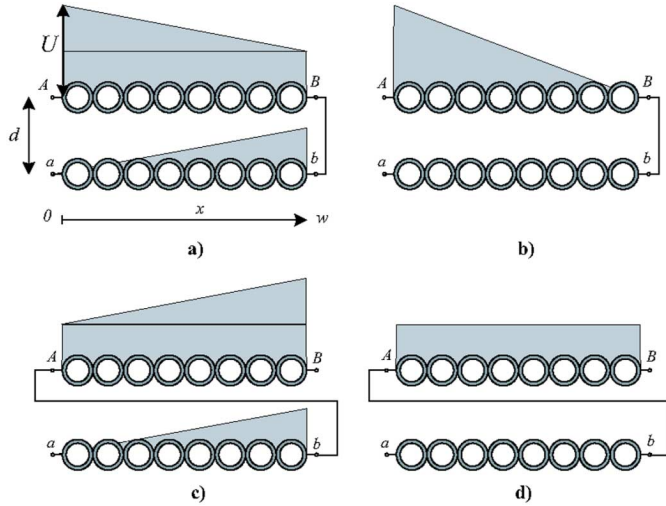


Fig. 11. Voltage distribution in dependence on the layers connection. Layers wound in opposite direction, (a), and (b) equivalent potential distribution. Layers wound in the same direction, (c), and (d) equivalent potential distribution. The terminal a is grounded.

according to the connection among terminals of adjacent layers, i.e., the winding strategy, the potential distribution along the turns varies and consequently so does the value of the layer-to-layer capacitance.

C. Effect of the Connection Between Adjacent Layers

An interesting way to derive the value of the equivalent capacitance when different connections of the layers are considered, is provided by the “Principle of Virtual Work” (PVW) [34, p.460]. If U is the voltage difference between two layers, as those depicted in Fig. 10, then the corresponding electrostatic energy W_ε stored between the layers is given by

$$W_\varepsilon = \frac{1}{2} \int_{\text{Vol}} D \cdot E dv = \frac{1}{2} C_{\parallel} U^2. \quad (22)$$

Consider the two possible connections between two adjacent layers, i.e., layers wound in opposite directions [see Fig. 11(a)] or in the same direction [see Fig. 11(c)].

According to the PVW, the stored electrostatic energy can be calculated by realizing that no matter what process is used to assemble the system, the final configuration (d and w) and the voltage distribution are the same. For the connection as in Fig. 11(a), that provides the equivalent voltage distribution shown in Fig. 11(b), the electric field is given by

$$E(x) = \frac{U}{d} \frac{x}{w} \quad (23)$$

and the electrostatic energy stored corresponding to this configuration is given by

$$\begin{aligned} W_\varepsilon &= \frac{1}{2} \int_{\text{Vol}} \varepsilon E^2(x) dv \\ &= \frac{1}{2} \varepsilon l d \frac{w}{d^2} \frac{U^2}{3} = \frac{1}{2} C_{\parallel} U^2 \\ &= \frac{1}{2} C_{\text{eq}} U^2 \end{aligned} \quad (24)$$

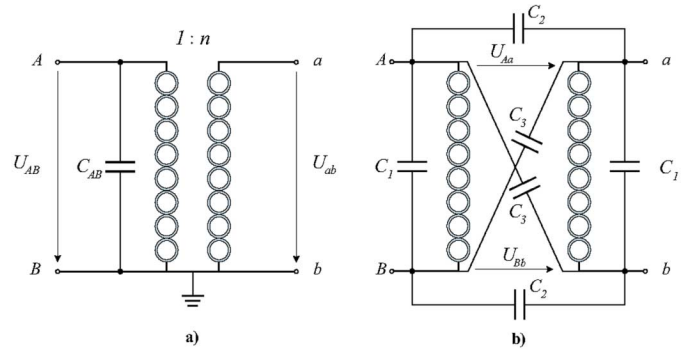


Fig. 12. (a) Equivalent capacitance C_{AB} of two coils wound in opposite direction, with voltage ratio $n = U_{ab}/U_{AB}$ and one terminal grounded. (b) Lumped capacitances C_1 , C_2 and C_3 associated with a 2-D distribution of the electric field for the configuration depicted in Fig. 10.

where ε is the equivalent dielectric constant of the media interposed between the layers, l the average turn length and C_{\parallel} is the static interlayer capacitance, (20). For the connection in Fig. 11(c), which provides the equivalent voltage distribution shown in Fig. 11(d), the electric field and the corresponding stored energy can be derived with the same procedure and are given, respectively, by

$$E(x) = \frac{U}{2d} \quad (25)$$

and

$$\begin{aligned} W_\varepsilon &= \frac{1}{2} \frac{C_{\parallel}}{4} U^2 \\ &= \frac{1}{2} C'_{\text{eq}} U^2. \end{aligned} \quad (26)$$

Thus, layers wound in the same direction show a lower equivalent capacitance C'_{eq} than the capacitance C_{eq} of layers wound in opposite direction and this is due to the different potential distribution corresponding to the two configurations.

D. Effect of the Voltage Ratio and Spacing Between Adjacent Layers

The voltage difference between adjacent layers or windings affects the value of the static capacitance. In Fig. 10 the ports AB and ab of two adjacent layers are shown. If the voltages U_{ab} and U_{AB} or U_{Aa} and U_{Bb} are known, the value of the capacitance at one port can be expressed by:

$$C = \frac{C_{\parallel}}{3U_{\text{ref}}^2} [(U_{Aa} + U_{Bb})^2 - U_{Aa}U_{Bb}] \quad (27)$$

where C_{\parallel} indicates the static layer-to-layer capacitance and U_{ref} is a reference voltage [7]. Lets now assume the connection shown in Fig. 12(a) of the two coils, a sketch of which is depicted in Fig. 10. If the voltage $U_{AB} = U_{ab}/n$ is taken as reference voltage for the calculation of the capacitance at the terminals AB according to (27), the capacitance C_{AB} shown in Fig. 12(a) is provided by

$$C_{AB} = \frac{C_{\parallel}}{3} (n-1)^2. \quad (28)$$

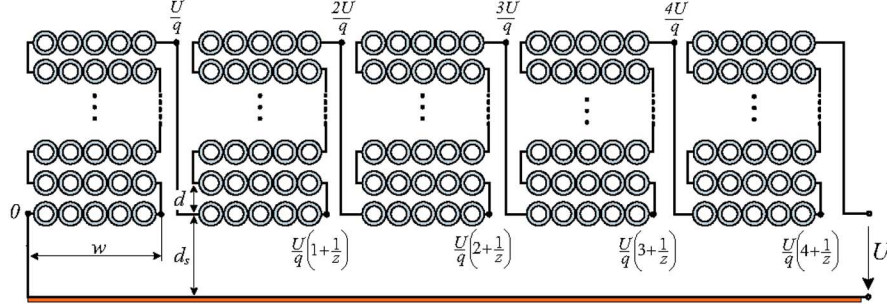


Fig. 13. Distribution of the voltage U across a coil of $q = 5$ sections and z layers per section; d indicates the inter-layer distance while d_s is the distance between the inner layers and the screen.

where n indicates the voltage ratio. Equation (27) is derived under the assumption of potential variation only between the layers.

If the variation of the voltage within the same layer of turns is considered as well, then the electric field has two components (E_x, E_y) rather than just E_x , as assumed so far. The equivalent circuit in Fig. 12(b) shows the six capacitances, of which two are linearly independent, that are associated with a 2-D electric field distribution for the winding architecture shown in Fig. 10. Such a field distribution is strongly dependent on the the distance d between adjacent layers; accordingly, the assumption of 2-D electric field distribution is more valid the larger the distance d . It can be easily proven [35], that these capacitances assume the following values:

$$\begin{aligned} C_1 &= -\frac{C_{11}}{6} \left(1 - 2\frac{d^2}{w^2}\right) \\ C_2 &= +\frac{C_{11}}{3} \left(1 - \frac{d^2}{2w^2}\right) \\ C_3 &= +\frac{C_{11}}{6} \left(1 + \frac{d^2}{w^2}\right). \end{aligned} \quad (29)$$

The equivalent capacitance C_{AB} of the two port system corresponding to the connection shown in Fig. 12(b), under the assumption of 2-D electric field distribution, is provided by

$$C_{AB} = (C_1 + C_3)(1 + n^2) + C_2(1 - n)^2. \quad (30)$$

By substituting the values (29) into (30), the capacitance C_{AB} becomes a function of the static interlayer capacitance C_{11} and of the geometric parameters d and w :

$$C_{AB} = \frac{C_{11}}{3}(1 - n)^2 + \frac{d^2}{3w^2}C_{11}(1 + n + n^2). \quad (31)$$

If the equivalent distance d (21) between two adjacent layers is small compared to the width w of each layer (see Fig. 10), then the (31), derived under the assumption of 2-D electric field distribution, can be simplified to (28). This equation corresponds to 1-D field distribution.

E. Capacitance Towards Screen

The capacitance against the screen is due to the electrostatic energy stored in the gap between the secondary winding and the screen. For this calculation, it is assumed that only the lower layers of the sections contribute to the capacitance, since the electric field between the screen and layers in front of the screen provides the major contribution to the electrostatic energy stored. The distribution of the voltage U across a coil of q sections and z layers per section is shown in Fig. 13. The energy stored between each section and the screen is calculated in a similar fashion as in [7] and then all contributions can be summed up to provide the total energy stored between the screen and the conductive layer opposite to the screen. Hence the resulting layer-to-screen capacitance C_{1s} assumes the following expression:

$$C_{1s} = \sum_{i=1}^q C_{1s,i} \frac{1}{q^2 z^2} \left(\frac{3z^2(i-1)^2 + 3z(i-1) + 1}{3} \right) \quad (32)$$

where $C_{1s,i}$ is the static capacitance between each section of width w and the screen, which can be calculated in a similar fashion as (20).

For a large number of sections q , the previous formula (32) can be simplified into

$$C_{1s} = \frac{C_{1s,i}q}{3} \quad (33)$$

where the capacitance $C_{1s,i}$ between each section and the screen can be assumed equal for all the sections, if the width w is the same for all sections (see Fig. 13). A good approximation for $C_{1s,i}$ (per unit of length) is given by

$$C_{1s,i} = \varepsilon_{\text{eqs}} \frac{2\pi w}{\ln\left(1 + \frac{d_s}{a}\right)} \quad (34)$$

where ε_{eqs} is the equivalent dielectric constant that accounts for the properties of the insulation of the wires faced to the screen and the air between the layer and screen. The parameter a is the

radial distance of the screen from the central axis (see Fig. 1) and d_s is the distance of the secondary from the screen (see Fig. 13).

V. EXPERIMENTAL RESULTS

In order to verify the consistency of the procedure for calculating the self-capacitance, measurements and calculations have been performed for three different transformers architectures. The high-voltage transformers possess the same construction characteristics (see Fig. 1) but different numbers of layers, sections and winding arrangements. The geometrical features of the transformers and the properties of the windings are shown in the Appendix.

If one refers all the contributions to the self-capacitance to primary side of the transformer, the capacitances of the secondary windings and the capacitances between secondary windings and screen have to be multiplied by a factor n^2 , where n is the transformer turns ratio (very large for step-up transformers) [35]. In light of this, the contribution of the primary and the inter-windings mutual capacitances (between primary and secondary) to the equivalent capacitance can be considered negligible.

The secondary winding impedance has been measured with an Agilent A294A impedance analyzer for the following two conditions. The measurement was first performed without the screen and the magnetic core. In this case the value of the first parallel-resonance frequency f_p , given by

$$f_p = \frac{1}{2\pi\sqrt{LC}} \quad (35)$$

is shifted to higher frequencies than for the cored system since the magnetizing inductance L without the core assumes a lower value. Secondly, the impedance was measured for the system comprising of the core and the screen (see Fig. 14). The measurement realized without the core and screen provides the self-capacitance of the winding while the measurement performed with connected screen and winding gives the total capacitance, i.e., the sum of the winding self-capacitance and the capacitance to the screen. From these latter two measurements, the capacitance towards the screen was calculated as the difference. Both measurements with and without core showed that the stray capacitance towards the core can be neglected since the screen is interposed between windings and core for these transformer architectures.

The connections of the secondary winding's terminal adopted during the impedance measurements for the transformers # 1 is shown in Fig. 15(a)–(b). This transformer has two secondary windings that are series connected in operation, with one terminal connected to the screen and grounded. Transformers # 2 and # 3 have only one secondary winding, with one terminal grounded and connected to the screen in normal operation [see Fig. 15(c)–(d)].

Table II shows the experimental and analytical results obtained for the three transformers. The winding self-capacitance has been calculated by substituting the formulas (20) into (18) and (19) and considering (24) or (26) according to the type of connection of the layers. The capacitance against the screen was calculated with (32), (33) and (34). For the transformer #

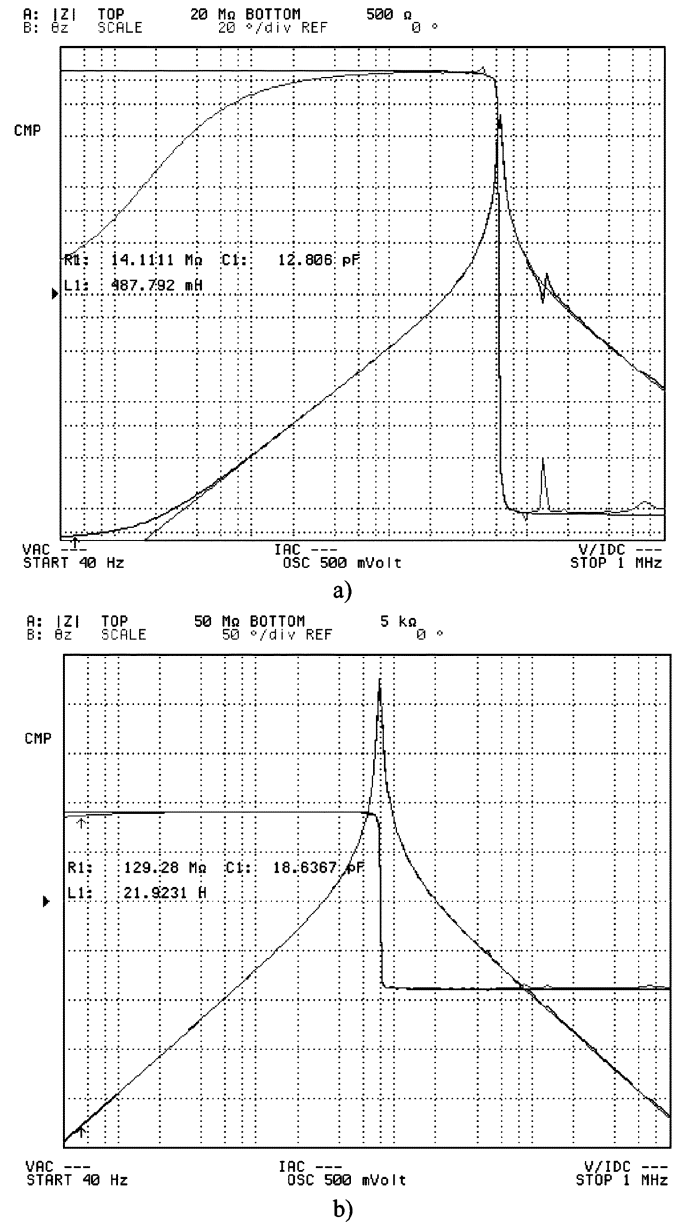


Fig. 14. Measured self-capacitance of the secondary winding without the screen and the core (a) and measured self-capacitance for the system comprising of the screen and the core for the transformer # 3 (b).

1 having two secondary windings, one of the secondaries has been short circuited during the measurement, to avoid the magnetic coupling between the two secondaries; moreover, the total self-capacitance is given by the sum of two times the winding self-capacitance and the capacitance to the screen.

From Table II it is evident that the relative error between calculated and measured self-capacitance is constant. The parameter that mostly affects the calculation of the winding self-capacitance is the equivalent distance d between wires (21). Furthermore, the analytical results have been obtained assuming that the turns of each layer are aligned as shown in Fig. 2(a). If the conductors were orthogonal, as shown in Fig. 2(b), the value of the static dc capacitance is two times the value obtained for aligned conductors [30].

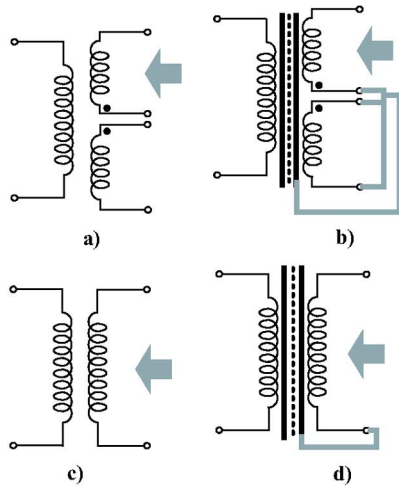


Fig. 15. Connections of the secondary winding's terminals adopted during the impedance measurement for transformers # 1, (a) and (b), and transformers # 2 and # 3, (c) and (d), respectively.

TABLE II
EXPERIMENTAL RESULTS [pF]

Transformer # 1			
	Calculated	Measured	Error (%)
Self-capacitance of secondary winding (2 Secondaries)	3.15	3.84	-17.97
Self-capacitance towards screen	8.06	9.96	-19.08
Total self-capacitance	14.36	17.64	-18.59
Transformer # 2			
	Calculated	Measured	Error (%)
Self-capacitance of secondary winding	3.97	4.84	-17.98
Self-capacitance towards screen	10.84	13.26	-18.25
Total self-capacitance	14.81	18.10	-18.18
Transformer # 3			
	Calculated	Measured	Error (%)
Self-capacitance of secondary winding	10.47	12.80	-18.20
Self-capacitance towards screen	4.75	5.84	-18.66
Total self-capacitance	15.22	18.64	-18.35

The capacitance value is therefore between two case limits with dependence on the the winding arrangement: lowest capacitance value for turns aligned and highest capacitance value for an orthocyclic packing. Since the aligned turns condition was assumed, then the results shown in Table II correspond to minimum capacitance values; the same assumption has been done for the calculation presented in Table I. A correct assessment of the mutual position of the turns can reduce the calculation error. For the transformers considered, the turns within each section of the windings are not exactly aligned but they are as well not orthogonally placed. A correcting factor k , defined as

$$1 < k < 2 \quad (36)$$

can be introduced and used to take into account the mutual position of the turns within a section. It was estimated between 1.1 and 1.3 for these transformers and this can be assessed depending on the angle α shown in Fig. 2. This factor, once mul-

tiplied by the calculated capacitance value, would compensate the calculation error.

The calculation of the capacitance due to screen is also affected by an error of -18% and this is due to the simplification made of modelling the static dc capacitance between winding and screen as an ideal cylindrical capacitor. This approximation is accurate if the secondary winding is divided into several sections with the same characteristics (33).

VI. CONCLUSION

This work presented a comprehensive procedure for calculating the self-capacitance of high-voltage transformers. Such transformers usually find application within isolated dc-to-dc converters where the transformer's self-capacitance and leakage inductance are used as elements of the resonant tank.

The analytical approach was selected over the FEM approach because there is a good tradeoff between speed in acquiring the results and their accuracy. The proposed procedure of calculation is based on a physical approach and equations for calculating the turn-to-turn, interlayer, section's and winding capacitances, respectively, were explained.

The approach and formulas presented in this paper can be used for wound components other than just step-up transformers. The influence of the core on the electric field distribution was analyzed and the dielectric characteristics of N87 ferrite grade extracted. Including the core's resistance in the equivalent circuit of the winding is important to correctly reproduce the frequency behavior. Moreover, the dependence of the value of a single layer capacitance on the number of turns was shown.

The two factors that are responsible for the error in the calculation are: the distance d between layers and the turns arrangement, either aligned or orthocyclic.

The principle of virtual work was used to show how different potential distributions influence the value of the static interlayer capacitance. It was proven that a six-capacitances equivalent model corresponding to 2-D electric field distribution can be reduced to a conventional single capacitance associated to the 1-D electric field distribution, if the equivalent distance d between layers or adjacent windings is small enough.

The experimental results show that the calculation's procedure is consistent for different transformer architectures and the error remains constant.

The proposed analysis of the electrostatic behavior of high-voltage transformer and the calculation procedure are important from a practical standpoint for three different purposes:

- reducing the capacitance value and hence the dielectric losses (by modifying for instance the winding arrangement);
- using the self capacitance of the transformer as an effective circuital parameter (integration);
- applying a strategy of capacitance cancellation, that already succeeded for other two port devices [36].

APPENDIX I

See Table III.

TABLE III
TECHNICAL SPECIFICATIONS OF THE TRANSFORMERS
USED FOR THE EXPERIMENTAL VALIDATION

Transformer # 1 with ER98 Core		
Outer diameter of secondary wire	$d_{e \max}$	0.472 mm
Insulation thickness	h	20 μm
Dielectric constant of insulation	ε	3.55
Number of turns per layer	n_t	5
Number of layers	z	10
Number of sections	q	5
Average turn length	l	$2\pi \cdot 26$ mm
Breath of each section	w	2.5 mm
Distance from screen	d_s	8 mm
Distance screen from axis	a	15.5 mm
Breath of screen	L	52 mm
Transformer # 2 with 72/65/39 Core		
Outer diameter of secondary wire	$d_{e \max}$	0.297 mm
Insulation thickness	h	16 μm
Dielectric constant of insulation	ε	3.55
Number of turns per layer	n_t	27
Number of layers	z	5
Number of sections	q	11
Average turn length	l	$2\pi \cdot 31.7$ mm
Breath of each section	w	4 mm
Distance from screen	d_s	10.9 mm
Distance screen from axis	a	18.5 mm
Breath of screen	L	81 mm
Transformer # 3 with U 93/76/20 Core		
Outer diameter of secondary wire	$d_{e \max}$	0.194 mm
Insulation thickness	h	11.5 μm
Dielectric constant of insulation	ε	3.55
Number of turns per layer	n_t	26
Number of layers	z	20
Number of sections	q	5
Average turn length	l	$2\pi \cdot 40$ mm
Breath of each section	w	5 mm
Distance from screen	d_s	15 mm
Distance screen from axis	a	21.5 mm
Breath of screen	L	41 mm

ACKNOWLEDGMENT

The authors wish to thank Dr. A. Massarini for providing relevant literature, Dr. M. Ciappa for his suggestions about the experimental setup, and J. Claassens for manuscript discussion.

REFERENCES

- [1] W. Lenz, "Calculation of the free period of a single layer coil," *Annal. Phys.*, vol. 43, pp. 749–97, 1914.
- [2] J. L. Thompson and S. A. Stigant, "Overvoltages in transformers due to the self-capacity of the windings," *Elect. Rev.*, vol. 76, pp. 25–37, 1915.
- [3] D. Maurice and R. H. Minns, "Very-wide band radio frequency transformers," *Wireless Eng.*, vol. 24, pp. 169, 209–177, 216, Jun./Jul. 1947.
- [4] R. Feldkeller, *Theory of Coils and Transformers*. Stuttgart, Germany: Hirzel Verlag, 1971.
- [5] P. A. Abetti, "Survey and classification of published data on the surge performance of transformers and rotating machines," *AIEE Trans.*, vol. 77, pp. 1403–1414, Dec. 1958.
- [6] H. Zuhrt, "Simple approximate formulas for the self capacitance of multi-layer coils," *Elektrotech. Zeitschrift*, vol. 55, pp. 662–665, Jul. 1934.
- [7] W. T. Duerdoth, "Equivalent capacitance of transformer windings," *Wireless Eng.*, vol. 23, pp. 161–167, Jun. 1946.
- [8] R. G. Meldhurst, "High-frequency resistance and self-capacitance of single layers solenoids," *Wireless Eng.*, vol. 24, pp. 35–43, Feb. 1947.
- [9] P. A. Abetti and F. J. Maginiss, "Natural frequencies of coils and windings determined by equivalent circuit," *AIEE Trans.*, vol. I, pp. 495–504, Jun. 1953.
- [10] R. C. Degeneff, "A general method for determining resonances in transformer windings," *IEEE Trans. Power App. Syst.*, vol. PAS-96, no. 2, pp. 423–430, Mar. 1977.
- [11] L. F. Casey, A. F. Goldberg, and M. F. Schlecht, "Issues regarding the capacitance of 1–10 MHz transformers," in *Proc. Appl. Power Electron. Conf. Expo*, Feb. 1–5, 1988, pp. 352–359.
- [12] S. Wang, F. C. Lee, and W. G. Odendaal, "Single layer iron powder core inductor model and its effects on boost PFC EMI noise," in *Proc. Power Electron. Spec. Conf.*, 2003, pp. 874–852.
- [13] L. Zhao, J. T. Strydom, and J. D. van Wyk, "Wide band modelling of integrated power passive structures: The series resonator," in *Proc. Power Electron. Spec. Conf.*, 2002, pp. 1283–1288.
- [14] A. Massarini and M. K. Kazimierczuk, "Self-capacitance of inductors," *IEEE Trans. Power Electron.*, vol. 12, no. 4, pp. 671–676, Jul. 1997.
- [15] T. Duerbaum and G. Sauerlander, "Energy based capacitance model for magnetic devices," in *Proc. Appl. Power Electron. Conf.*, 2001, vol. 1, pp. 109–115.
- [16] B. Ackermann, A. Lewalter, and E. Waffenschmidt, "Analytical modelling of winding capacitances and dielectric losses for planar transformers," in *Proc. Comput. Power Electron. Workshop*, 2004, vol. 1, pp. 2–9.
- [17] T. Duerbaum, "Capacitance model for magnetic devices," in *Proc. Power Electron. Spec. Conf.*, 2000, vol. 3, pp. 1651–1656.
- [18] H. Y. Lu, J. Zhu, S. Y. R. Hui, and V. S. Ramseden, "Measurement and Modeling of stray capacitances in high frequency transformers," in *Proc. Power Electron. Spec. Conf.*, 1999, pp. 763–769.
- [19] H. Y. Lu, J. G. Zhu, and S. Y. R. Hui, "Experimental determination of stray capacitances in high-frequency transformers," *IEEE Trans. Power Electron.*, vol. 18, no. 5, pp. 1105–1112, Sep. 2003.
- [20] F. Cavalcante and J. W. Kolar, "Design of a 5 kW high-output voltage series-parallel resonant DC–DC converter," in *Proc. Power Electron. Spec. Conf.*, 2003, pp. 1807–1814.
- [21] F. Cavalcante and J. W. Kolar, "Small-signal model of a 5 kW high-output voltage capacitive-loaded series-parallel resonant DC–DC converter," in *Proc. Power Electron. Spec. Conf.*, 2005, pp. 1271–1277.
- [22] S. Johnson, A. Witulski, and R. Erickson, "Comparison of resonant topologies in high-voltage dc applications," *IEEE Trans. Aerosp. Electron. Syst.*, vol. AES-24, no. 3, pp. 263–274, May 1988.
- [23] J. Sun, M. Nakaoka, and H. Takano, "High-voltage transformer parasitic resonant PWM DC–DC high power converters and their performance evaluations," *Proc. ISIE*, pp. 572–577, 1997.
- [24] B. Tala-Ighil, J.-M. Noybe-Yome, P. Gouton, and C. Glaize, "On the utilization of the transformers parasitic capacitances as a resonant element in high-voltage converters operating above resonance with variable frequency," *Colloq. Stat. Power Conv.*, vol. 3, pp. 1–5, 1992.
- [25] J. Collins, "An accurate method for modelling the transformer winding capacitances," in *Proc. Ind. Electron. Conf.*, 1990, pp. 1094–1099.
- [26] M. Albach and J. Lauter, "The winding capacitance of solid and Litz wires," in *Proc. Eur. Power Electron. Conf.*, 1997, pp. 1–5.
- [27] J. Koch, "Berechnung der Kapazität von Spulen, insbesondere in Schalenkernen," *Volvo Berichte*, vol. 14, no. 3, pp. 99–119, 1968.
- [28] L. Dalessandro, W. G. Odendaal, and J. W. Kolar, "HF characterization and non linear modelling of a gapped toroidal magnetic structure," *IEEE Trans. Power Electron.*, vol. 21, no. 5, pp. 1167–1175, Sep. 2006.
- [29] Epcos, "EPCOS, Ferrites," Tech. Rep., 2005 [Online]. Available: www.epcos.com
- [30] E. C. Snelling, *Soft Ferrites—Properties and Applications*, 2nd ed. London, U.K.: Butterworth, 1988.
- [31] F. G. Brockmann, P. H. Dowling, and W. G. Steneck, "Dimensional effects resulting from a high dielectric constant found in a ferromagnetic ferrite," *Phys. Rev.*, vol. 77, no. 1, pp. 85–93, 1950.
- [32] G. Grandi, M. K. Kazimierczuk, A. Massarini, and U. Reggiani, "Stray capacitances of single-layer solenoid air-core inductors," *IEEE Trans. Ind. Appl.*, vol. 35, no. 5, pp. 1162–1168, Sep./Oct. 1999.
- [33] E. Labouré, F. Costa, and F. Forest, "Current measurement in static converters and realization of a high frequency passive current probe," in *Proc. Eur. Power Electron. Conf.*, 1993, pp. 478–483.
- [34] M. Zahn, *Electromagnetic Field Theory—A Problem Solving Approach*. Melbourne, FL: Krieger, 2003.
- [35] E. Laveuve, J.-P. Keradec, and M. Bensoam, "Electrostatic of wound components: Analytical results, simulation and experimental validation of the parasitic capacitance," in *Proc. Ind. Appl. Soc. Annu. Meeting*, Oct. 1991, vol. 2, pp. 1469–1475.
- [36] R. Chen, J. D. van Wyk, S. Wang, and W. G. Odendaal, "Application of structural winding capacitance cancellation for integrated EMI filters by embedding conductive layers," in *Proc. Ind. Appl. Soc.*, 2004, pp. 2679–2686.
- [37] L. Dalessandro, F. Cavalcante, and J. W. Kolar, "Calculation of the Stray Capacitance of High-Voltage Transformers," ETH Zurich, Zurich, Switzerland, Int. Rep. 03/04, Mar. 2004.



Luca Dalessandro (S'02) was born in Italy on April 29, 1978. He received the M.Sc. degree (with first class honors) in electrical engineering from the Politecnico di Bari, Bari, Italy, in 2001 and is currently pursuing the Ph.D. degree in electrical engineering at the Swiss Federal Institute of Technology (ETH) Zurich, Switzerland.

From 2001 to 2002, he was Researcher at the Max-Planck-Institute for Mathematics in the Sciences (MPI-MIS), Leipzig, Germany. From 2002 to 2006, he was a Research and Teaching Assistant at the Power Electronics Systems Laboratory (PES), ETH Zurich. In the summer of 2006, he joined the NSF Engineering Research Center for Power Electronics Systems (CPES), Virginia Polytechnic Institute and State University, Blacksburg, as a Researcher. He is also an Adjunct Faculty Member of the Bradley Department of Electrical and Computer Engineering, Virginia Tech, for which he teaches an advanced course on electromagnetic fields. His research interests include three-phase converters, electromagnetics, EMC and continuum electromechanics.

Mr. Dalessandro is a Registered Professional Engineer in Italy.



Fabiana da Silveira Cavalcante (S'02) was born in Itabuna, Bahia, Brazil, in 1976. She received the B.S. and M.S. degrees in electrical engineering from the Federal University of Santa Catarina, Florianópolis, Brazil, in 2000 and 2001, respectively, and the Ph.D. degree from the Swiss Federal Institute of Technology Zurich (ETH), Zurich, Switzerland, in 2006.

Since January 2006, she has been with ABB Switzerland, Ltd., Turgi, Switzerland, where she is a Development Engineer for Traction Products.

Her research interests include the modeling and control of resonant dc–dc converters, electronic ballasts, soft switching techniques, and three-phase converter systems for railway applications.



Johann W. Kolar (SM'04) received the Ph.D. degree (with highest honors) in industrial electronics from the University of Technology, Vienna, Austria.

Since 1984, he has been with the University of Technology, Vienna, and has been teaching and working in research in close collaboration with international industry in the fields of high performance drives, high frequency inverter systems for process technology, and uninterruptible power supplies. He has proposed numerous novel converter topologies, e.g., the Vienna rectifier and the three-phase ac–ac sparse matrix converter concept. He has published over 200 scientific papers in international journals and conference proceedings and has filed more than 50 patents. He was appointed Professor and Head of the Power Electronic Systems Laboratory, Swiss Federal Institute of Technology (ETH), Zurich, in 2001. Since 2002, he has been an Associate Editor of the *Journal of Power Electronics* of the Korean Institute of Power Electronics and a member of the Editorial Advisory Board of the *IEEE Transactions on Electrical and Electronic Engineering*. The focus of his current research is on acac and ac–dc converter topologies with low effects on the mains, e.g., for power supply of telecommunication systems, more-electric-aircraft applications, and distributed power systems in connection with fuel cells. Further main areas of research are the realization of ultracompact intelligent converter modules employing the latest power semiconductor technology (SiC), novel concepts for cooling and EMI filtering, multiphysics/multiscale simulation, pulsed power, bearingless motors, and power MEMS.

Dr. Kolar is a member of the IEEJ and of Technical Program Committees of numerous international conferences in the field (e.g., Director of the Power Quality Branch of the International Conference on Power Conversion and Intelligent Motion). From 1997 through 2000, he served as an Associate Editor of the IEEE TRANSACTIONS ON INDUSTRIAL ELECTRONICS and since 2001 as an Associate Editor of the IEEE TRANSACTIONS ON POWER ELECTRONICS.